Supporting Information

Praper et al. 10.1073/pnas.1107473108

SI Materials and Methods

Native human perforin (PFN) was isolated as described by Froelich et al. (1), and was devoid of impurities according to a silver-stained SDS-PAGE gel (Fig. S7). Granzyme B was purified as described in ref. 2 and labeled by Alexa488. Pneumolysin was purified according to Gilbert et al. (3) and lysenin according to Bruehn et al. (4). Cholesterol, 1,2-dioleoyl-*sn*-glycero-3-phosphocholine (DOPC), and 1,2-diphytanoyl-*sn*-glycero-3-phosphocholine (DPhPC) were from Avanti Polar Lipids. Rhodamine B 1,2-dihexadecanoyl-*sn*-glycero-3-phosphoethanolamine, triethylammonium salt (rDHPE) and 1,1′-dioctadecyl-3,3,3′,3′-tetramethylindodicarbocyanine perchlorate ($DilC_{18}$) were from Invitrogen. Dextrans labeled with FITC (4, 10, 70 kDa) were from Sigma. FITC-labeled monoclonal antibodies (anti-PFN δG9 and antiglycophorin) were from Santa Cruz. All other chemicals were from Sigma or Merck.

Electroformation of GUVs. GUVs were prepared by electroformation as described in ref. 5 with modifications. The lipids were dissolved in chloroform/methanol (2:1, vol/vol) to 1 mM final concentration. Twenty-five microliters of the lipid solution was spread onto a pair of Pt electrodes and dried under reduced pressure for 2 h. Electrodes (dimensions, φ: 1 mm, length 34 mm, spacing between electrodes 4 mm) were then placed into a vial filled with sucrose buffer (295 mM sucrose, 1 mM Hepes, 0.25 mM Ca). Alternating current was applied with a functional generator (GW Instek GFG-3015). The protocol for electroformation was as follows: 2 h of 4 V/10 Hz; 15 min of 2 V/5 Hz; 15 min of 1 V/2.5 Hz; 30 min of 1 V/1 Hz. Giant unilamellar vesicles (GUVs) were sedimented with the glucose buffer (295 mM glucose, 1 mM Hepes, 0.25 mM $CaCl_2$). The buffer was then exchanged by gentle pipetting with 150 mM NaCl, 20 mM Hepes, 0.25 mM $CaCl_2$, pH 7.4. GUVs were then divided into aliquots containing approximately equal amount of vesicles.

Preparation of Erythrocyte Membranes. Blood (group O) was collected from a healthy volunteer, placed in EDTA-containing tubes (Vacuette, Greiner BioOne) and washed with 140 mM NaCl, 5 mM Na_2HPO_4, pH 8.0. Erythrocytes were lysed by 5 mM Na_2HPO_4, pH 8.0, incubated 5 min on ice and centrifuged 20 min at 25,000 × *g* at 4 °C. Membranes were then separated from the supernatant, washed several times with water, and adjusted to a phospholipid concentration of 0.5 mg/mL. Phospholipid concentration was determined by LabAssay Phospholipid (Wako) according to the manufacturer's instructions. Solution of $DilC_{18}$ in DMSO (1 mg/mL) was added to membranes at a ratio 1:100 (vol/vol). Sixteen microliters of labeled membranes were then spread onto a pair of Pt electrodes and dried under reduced pressure overnight. Electroformation was performed as described above.

GUV Imaging Using Fluorescence Microscopy. Six microliters of GUV suspension was mixed with 0.5 or 1 μL of PFN and 0.5 μL of dextran. Final concentrations were 12 nM (PFN), 0.1 mM (D4), 0.03 mM (D10), or 0.01 mM (D70). For immunodetection 6 μL of GUV suspension was mixed with PFN to 12 nM final concentration and incubated for 10 min at 25 °C. Afterward, 1 μL of anti-PFN δG9-FITC was added and the mixture was incubated at 25 °C for a minimum of 30 min before microscopy. For the isotype control we used antiglycophorin-FITC-labeled antibody (IgG2b isotype). The final concentration of both antibodies used was 200 nM. In preliminary immunodetection studies we removed the anti-PFN antibody by gentle pipetting of a fresh buffer, but many GUVs were ruptured during this procedure. Because there was qualitatively no difference when the washing step was omitted, we did not remove the anti-PFN antibodies in the experiments shown in the manuscript. Fluorescence and differential interference contrast microscopy (DIC) were performed on an AxioImager Z1 (Carl Zeiss) equipped with an ApoTome for recording of optical sections (grid-confocal microscopy) and 100W HBO mercury arc illumination. FITC-labeled dextrans and antibodies were observed with a 450–490 nm band pass excitation and a 515 nm long pass emission filter. The membranes of the GUV-containing rDHPE were observed with a 546/12 nm band pass excitation and a 590 nm long pass emission filter. Series of Z-stack images for three-dimensional (3D) reconstitution (Fig. 1*E*) and immunodetection (Fig. 3*B*) were recorded by confocal laser-scanning microscopy on a Leica TCS SP5 laser-scanning microscope, mounted on a Leica DMI 6000 CS inverted microscope (Leica Microsystems). An HCX plan apo x63 (N.A., 1.4) oil immersion objective was used. Probes (D10 and FITC-labeled antibodies) were excited with the 488 nm line of an argon laser. Fluorescence emission was detected from 500 to 530 nm. The rDHPE in the GUV membranes was excited with the 543 nm line of the argon laser. Fluorescence emission was detected from 605 to 650 nm.

Surface Plasmon Resonance. Surface plasmon resonance experiments were performed as described (6) by using a Biacore X and L1 sensor chip (GE Healthcare). Binding to red blood cell ghosts was done as described previously (7). Ghosts were immobilized on the surface of the sensor chip to saturation in 20 mM Hepes, 150 mM NaCl, pH 7.4, and including 1 mM $CaCl_2$ or 1 mM EDTA. PFN was injected for 1 min at a flow rate of 10 μL/min and the dissociation was followed for 3 min.

Cryo-EM. Four hundred microliters of 10 mg/mL DOPC in chloroform (Avanti Polar Lipids) and 40 μL of 25 mg/mL plant cholesterol in chloroform (Avanti Polar Lipids) were dried on a clean Pyrex tube under argon. Residual chloroform was removed by overnight desiccation in a desicator attached to a VARIO-SP Diaphragm Pump (Vacuubrand). The lipid film was then hydrated by addition of 1 mL liposome buffer (20 mM Hepes, 150 mM NaCl, 250 μM $CaCl_2$ pH 7.4) at 50 °C followed by vigorous vortexing, giving an approximately 5 mg/mL lipid dispersion. After ten freeze-thaw cycles alternating between liquid nitrogen, a 50 °C water bath and a 1 min vortexing step, the dispersion was extruded 11 times with a Mini Extruder (Avanti Polar Lipids) through a Whatman polycarbonate membrane with a pore diameter of 100 nm. Liposomes were used immediately after preparation. PFN was added to liposomes at a final concentration of 10–20 ng/μL, and incubated at either room temperature or 37 °C. If the latter, then the liposomes and PFN were individually preincubated at 37 °C. Incubation times varied from 5 s to 5 min: Both pores and invaginated liposomes were observed at all time points (see ref. 8 for pore analysis). The number of pores was accentuated by longer incubations and 37 °C temperature, the presence of PFN at invaginations by shorter incubations. As a control for the effect of PFN itself we incubated a mixture of PFN buffer and large unilamellar vesicles (LUVs) at the same volume ratios used for samples containing PFN. Samples were flash-frozen in liquid ethane on 300 mesh lacy carbon grids and imaged using an FEI F30 FEG cryoelectron microscope operating at liquid nitrogen temperatures. Images were captured on SO-163 film (Kodak) and scanned using a Zeiss SCAI scanner.

Micrographs were corrected for their contrast transfer function (CTF) using CTFFIND3 (9) and EMAN (10). Images of pores and invaginations were individually boxed using the EMAN suite program BOXER, and subjected to image alignment and analysis using IMAGIC software (11).

Planar Lipid Bilayer Experiments and Membrane Area Measurements. Solvent-free planar lipid membranes (PLM) were formed over a 100–180-μm diameter hole sparkling drilled in a 25-μm thick Teflon septum thus separating two compartments, as described in ref. 12. The two Teflon chambers had a volume of 2 mL. Nanomolar concentrations of PFN (~0.5 nM) were added to the *cis* side of a stable preformed bilayer. All experiments were performed in symmetric conditions, using a buffer comprising 100 mM KCl, 20 mM Hepes, 0.1 mM $CaCl_2$, pH 7.4 in both chambers. A defined voltage, generally +40 mV, was applied to the *cis* side across the membrane, the *trans* side was grounded. The current across the bilayer was measured, and the conductance (G) was determined as follows: $G(\mathrm{pS}) = I(\mathrm{pA})/V(V)$, where I is the current through the membrane and V is the applied transmembrane potential. Macroscopic currents were recorded by a patch clamp amplifier (Axopatch 200, Axon Instruments). A PC equipped with a DigiData 1200 A/D converter (Axon Instruments) was used for data acquisition. The current traces were filtered at 0.5 kHz and acquired at 2 kHz by the computer using Axoscope 8 software (Axon Instruments). All measurements were performed at 24 °C.

The surface (A) of a PLM is related to its capacity (C_m) by the following equation (12):

$$A(\mathrm{nm}^2) = C_m(\mathrm{pF})d(\mathrm{nm})/(\epsilon_r\epsilon_0)(\mathrm{pF/nm}),$$

where d is the membrane thickness, $\epsilon_0 = 8.85 \times 10^{-9}$ pF/nm is the permittivity of free space and $\epsilon_r = 2.1$ is the dielectric constant of the membrane. For a membrane of defined lipids, where its thickness does not change during the experiment, membrane capacitance is therefore directly related to the membrane area. The additional lipids necessary for the increase of the membrane area were probably obtained from the excess lipids present on the septum surface and/or into the annulus region (13). Membrane capacity was measured via the ramp-based method, similarly to what is described in Schmitt and Koepsell (14). Paired ramps (total length 40 ms; from 0 to 5 mV then back to 0 mV) were applied every 0.4 s with a function generator (Agilent 33220A) (see Fig 4*A*, *Inset*). Membrane capacitance measurements were performed automatically by a script used during offline analysis, integrating the currents flown during the two voltage ramps and divided by the voltage change, as described in ref. 14.

The membrane capacity (C_m) was obtained by subtracting the capacity of the septum, which is 30 pF in our conditions. As a working test for the whole setup for recording changes in membrane capacitance, we subjected a stable preformed PLM to a hydrostatic pressure by increasing the water level into one compartment only (13). As expected, the hydrostatic pressure caused an increase in the membrane capacitance, until the membrane eventually brakes. This capacitance increase occurred independently of the compartment where the water level was raised and returned to zero after reestablishing the isobaric conditions.

Live Cell Imaging. Jurkat cells (15) were cultured in 75 mL flasks with RPMI medium 1640, 10% FCS, 1.5% L-glutamine and 1.5% penicillin and streptomycin. A few days prior to imaging the cell cultures were passaged by 15% of the primary cell culture being transferred to new media, so that the cells could be imaged nearer a log growth phase. Prior to imaging 1 mL of the cell culture was washed three times in HBS buffer (20 mM Hepes, 150 mM NaCl, pH 7.4), and spun down between washes at 1,000 rpm (170 × g) for 3 min. After removing the supernatant, the cells were placed in 1 mL of HBS with 1.25 mM $CaCl_2$ (HBS/$CaCl_2$ buffer) and resuspended by pipette and 3 s on a vortex shaker. The cell suspension was transferred to a PAA Labs 3.5 cm confocal petri dish, with the cell buffer filling the middle well, immediately above the glass coverslip. About 0.01 μL of CellMask PM Orange (Invitrogen red fluorescence emission cell membrane marker) and 0.5 μL of SYTOX Green (Invitrogen green fluorescence emission cell viability marker) were added to the HBS/$CaCl_2$ buffered cell culture a few minutes before imaging.

The PAA Labs petri dish was immediately transferred to a Zeiss Pecon XL3 large stage incubator with Pecon Labtek heated insert, attached to an Axiovert 200 M microscope on a Zeiss 510 MetaHead laser-scanning confocal system. The stage incubator temperature was set to 37 °C. HeNe laser 453 nm 1.2 mW laser excitation power was set to 5.0% and Argon laser 488 nm 30 mW laser excitation power set to 0.5%, to minimize light damage to the cells during imaging. After 5 min in the incubator chamber the petri dish lid was removed and a time-lapse started, set to continuous DIC transmission and red/green fluorescence imaging, with one scan every 13 s, at 1,024 × 1,024 pixels, with 2× averaging applied. Time-lapse video images were acquired using a Zeiss 63 × 1.4 N.A. Plan Apochromat DIC oil immersion objective set to 1× zoom, i.e., 630× magnification.

Initially the PFN was added directly to 400 μL cells in HBS/1.25 mM $CaCl_2$ buffer, typically in 0.1 to 2.6 μL volumes. It became clear that using this protocol the effects of the PFN were localized to the area where the concentrated PFN was pipetted in, and the effective concentration at work was therefore unknown. To ensure better mixing with the cell media and a more accurate final PFN concentration across the cell culture, the PFN was subsequently prediluted in HBS and then 200 μL of that added to 200 μL cells in HBS/1.25 mM $CaCl_2$ buffer (final Ca^{2+} concentration 0.625 mM). This procedure appeared to significantly improve PFN mixing with the cells across the petri dish, i.e., almost all the cells in the petri dish were affected, rather than localized pockets at the point of pipetting. To show calcium dependence of invagination formation we diluted the PFN prior to addition to cells with HBS 4 mM EDTA so that the final EDTA concentration in the mix of cells and PFN was 2 mM. Pneumolysin and lysenin were diluted to 0.2 μM and 36 μM, respectively, in HBS prior to mixing with equal volumes of Jurkat cells in HBS 1.25 mM $CaCl_2$, as before.

PFN was added at approximately 1 min into the time-lapse sequence at varying concentrations. The time-lapse was continued up to 30 min post addition of PFN, with a maximum of 140 field images captured. The PFN solution was quickly pipetted in one drop at a time in the approximate area of the point of focus —this procedure took around 4 s. Final PFN concentrations in the 400 uL of cell culture ranged from 48 to 1,000 ng mL^{-1}. Control time-lapse sequences were taken using 200 μL HBS added to 200 μL HBS/$CaCl_2$ buffered cell culture with no PFN. These controls demonstrated that over 100 continuous images could be acquired at these confocal settings before the cells being imaged were visibly adversely affected by the laser light.

The protocol for rotenone and azide-mediated depletion of ATP from the target cells was as follows. Rotenone (Sigma) was made up in a stock solution at 5 mM in DMSO. It was preincubated with cells for 1 h at a concentration of 0.1 mM in 200 μL HBS/$CaCl_2$ and then diluted with an equal volume of PFN at 0.58 ng/μL in 200 μL HBS so that the final concentration of PFN was 0.29 ng/μL. For the control cells without PFN the same protocol was followed except that the cells were mixed with an equal volume of 200 μL HBS without PFN prior to imaging. Azide was made up in a stock solution of 10% wt/vol. It was incubated with cells in 200 μL HBS/$CaCl_2$ buffer at 3.25% wt/vol

and then diluted with an equal volume of 200 μL HBS with 0.58 ng/μL PFN prior to imaging. Cells were prepared as described above for the imaging without ATP depletion.

Microscope images were acquired using LMS 510 v4.2 confocal software and the time-lapse videos were visualized/exported using Zeiss LMS browser v4.2.

1. Froelich CJ, Turbov J, Hanna W (1996) Human perforin: Rapid enrichment by immobilized metal affinity chromatography (IMAC) for whole cell cytotoxicity assays. *Biochem Biophys Res Commun* 229:44–49.
2. Froelich CJ, et al. (1996) New paradigm for lymphocyte granule-mediated cytotoxicity. Target cells bind and internalize granzyme B, but an endosomolytic agent is necessary for cytosolic delivery and subsequent apoptosis. *J Biol Chem* 271:29073–29079.
3. Gilbert RJC, et al. (1999) Studies on the structure and mechanism of a bacterial protein toxin by analytical ultracentrifugation and small-angle neutron scattering. *J Mol Biol* 293:1145–1160.
4. Bruhn H, Winkelmann J, Andersen C, Andrä J, Leippe M (2006) Dissection of the mechanisms of cytolytic and antibacterial activity of lysenin, a defence protein of the annelid *Eisenia fetida*. *Dev Comp Immunol* 30:597–606.
5. Peterlin P, Arrigler V (2008) Electroformation in a flow chamber with solution exchange as a means of preparation of flaccid giant vesicles. *Colloids Surf B* 64:77–87.
6. Anderluh G, Besenicar M, Kladnik A, Lakey JH, Macek P (2005) Properties of nonfused liposomes immobilized on an L1 Biacore chip and their permeabilization by a eukaryotic pore-forming toxin. *Anal Biochem* 344:43–52.
7. Bakrac B, et al. (2008) Molecular determinants of sphingomyelin specificity of a eukaryotic pore-forming toxin. *J Biol Chem* 283:18665–18677.
8. Praper T, et al. (2011) Human perforin employs different avenues to damage membranes. *J Biol Chem* 286:2946–2955.
9. Mindell JA, Grigorieff N (2003) Accurate determination of local defocus and specimen tilt in electron microscopy. *J Struct Biol* 142:334–347.
10. Ludtke SJ, Baldwin PR, Chiu W (1999) EMAN: Semiautomated software for high-resolution single-particle reconstructions. *J Struct Biol* 128:82–97.
11. van Heel M, Harauz G, Orlova EV, Schmidt R, Schatz M (1996) A new generation of the IMAGIC image processing system. *J Struct Biol* 116:17–24.
12. Dalla Serra M, Menestrina G (2000) Characterization of molecular properties of pore-forming toxins with planar lipid bilayers. *Methods Mol Biol* 145:171–188.
13. Benz R, Frohlich O, Lauger P, Montal M (1975) Electrical capacity of black lipid films and of lipid bilayers made from monolayers. *Biochim Biophys Acta* 394:323–334.
14. Schmitt BM, Koepsell H (2002) An improved method for real-time monitoring of membrane capacitance in *Xenopus laevis* oocytes. *Biophys J* 82:1345–1357.
15. Schneider U, Schwenk H, Bornkamm G (1977) Characterization of EBV-genome negative null and T cell lines derived from children with acute lymphoblastic leukemia and leukemic transformed non-Hodgkin lymphoma. *Int J Cancer* 19:621–626.

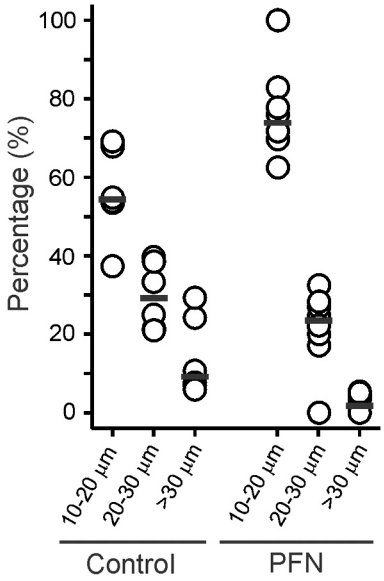

Fig. S1. Size distribution of GUVs in the absence and presence of PFN. The diameter of the vesicles was checked for the control GUVs (Control) and GUVs in the presence of 12 nM PFN (PFN). Data for six or eight experiments are presented for control or PFN, respectively. In total, we analyzed 382 and 368 GUVs for the control and PFN, respectively. The median is shown by a horizontal line.

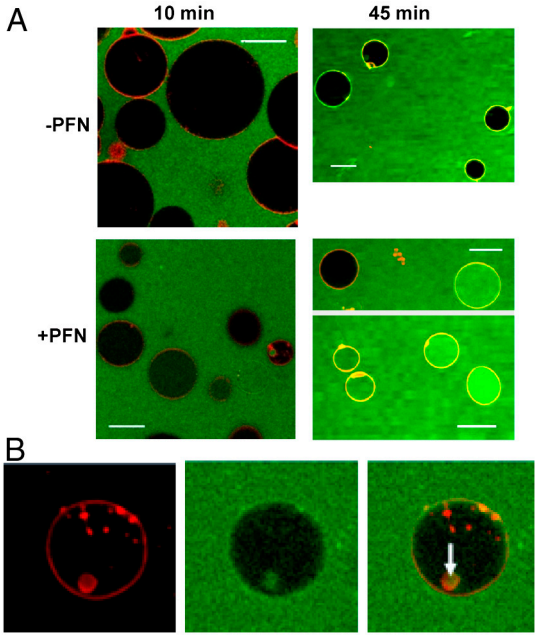

Fig. S2. Granzyme transfer into GUVs through pores and invaginations. Granzyme transfer across perforin pores is slow (*A*). Mixing GUVs together with perforin and Alexa488-labeled granzyme B: Transfer of granzyme B was very limited after 10 min but clear after 45 min of incubation. However granzyme B was found concentrated within invaginations (arrowed) already after 5 min incubation with perforin and granzyme B together (*B*).

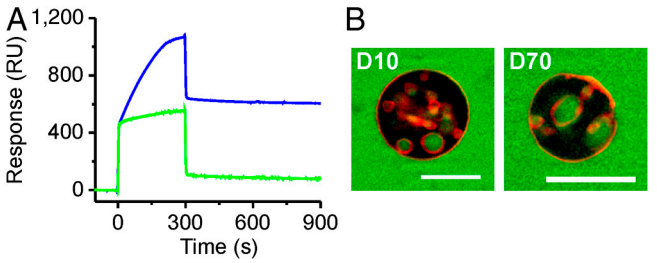

Fig. S3. Binding to red blood cell ghosts membranes in invagination formation in GUVs prepared from red blood cell membranes. (*A*) Binding of 50 nM PFN to human erythrocyte ghosts immobilized on the surface of L1 sensor chip in the presence of 1 mM $CaCl_2$ (blue) or 1 mM EDTA (green). (*B*) Secondary vesicle formation in GUVs prepared from erythrocyte ghosts and induced by the presence of 12 nM PFN. Scale bar in all panels is 20 μm.

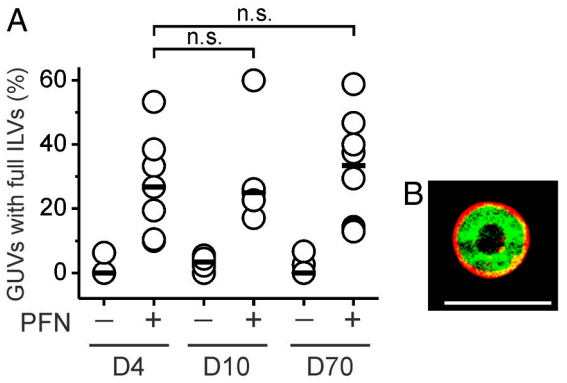

Fig. S4. The formation of invaginations in the presence of different dextranes. (*A*) The formation of intraluminal vesicles (ILVs) in the presence of fluorescent dextrans of different size in the absence and presence of 12 nM perforin. The data for 12 nM perforin in the presence of 0.25 mM $CaCl_2$ are presented. (*B*) Formation of ILV in the presence of 12 nM PFN and 0.25 mM $CaCl_2$. D70 was encapsulated during electroformation and GUVs were washed with addition of buffer without dextran. Not significant, n.s.

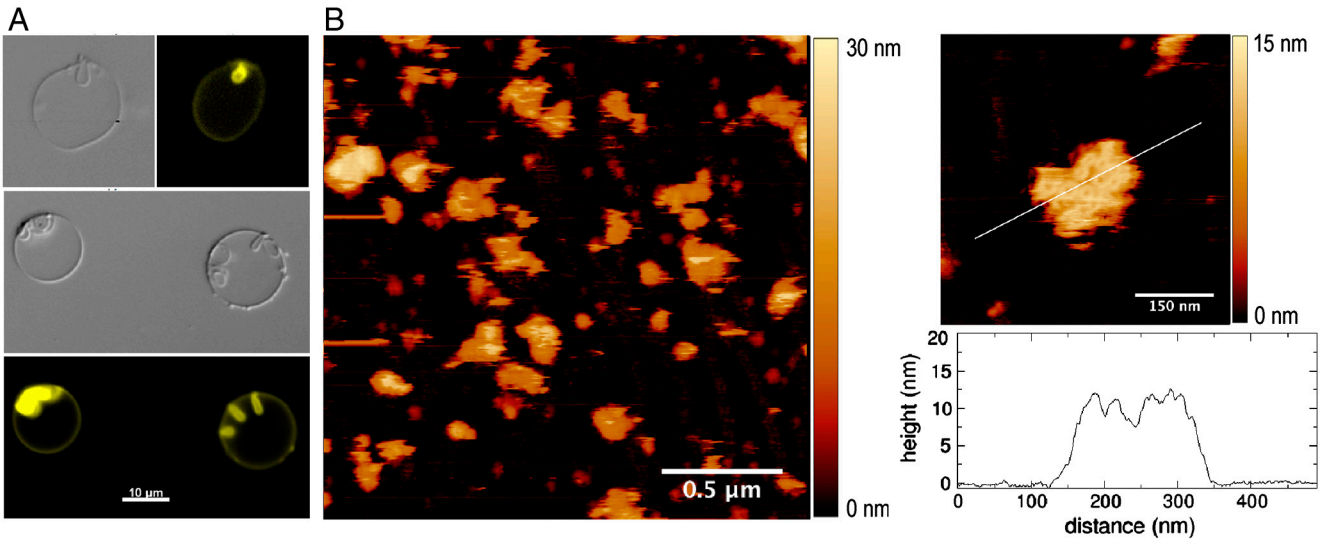

Fig. S5. Clustering of PFN on membranes. The clustering of human perforin on GUVs (*A*) and supported bilayers (*B*) composed of dioleoyl phosphatidylcholine and cholesterol (20 mol %). In *A* perforin was stained as described in the experimental section of the paper. Atomic force microscopy imaging was used for *B*. Supported lipid bilayers were prepared by the liposome fusion method, following the procedure describe by Tamm and McConnell (1). Atomic force microscopy (AFM) images have been taken in semicontact mode with a Cypher (Asylum Research) AFM equipped with a droplet cantilever holder. Olympus TR400 cantilevers have been used, driven approximately at 7.5 kHz. Image acquisition was performed by AFM software Igor Pro 6.12A (WaveMetrics, ZDA) and Gwydion 2.20. The concentration of perforin used was 12 nM.

1 Tamm LK, McConnell HM (1985) Supported phospholipid bilayers. *Biophys J* 47:105–113.

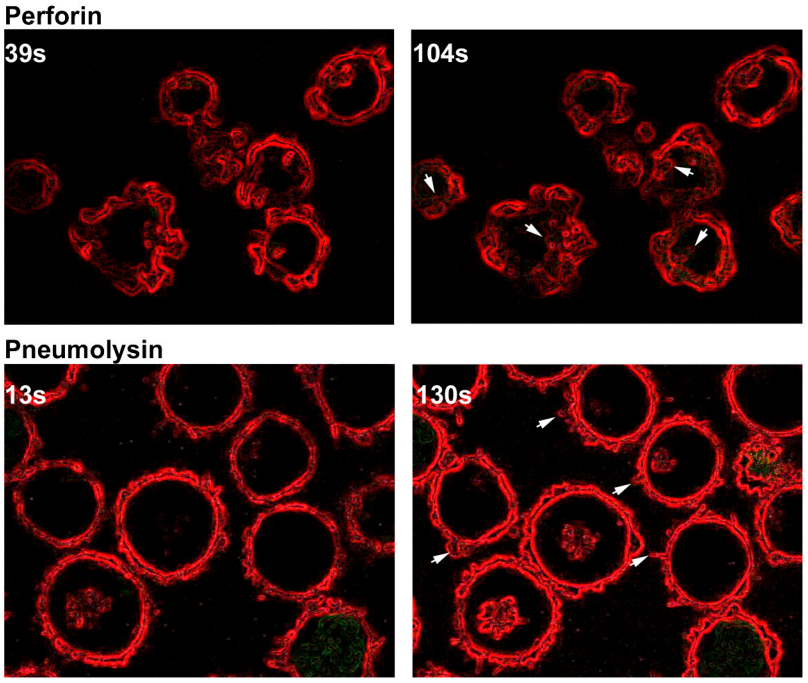

Fig. S6. Invaginations formed in Jurkat cells. Close-up images of edge-enhanced Jurkat cells from Fig. 4 *A* and *D* and Movies S2 and S8, showing changes in membrane morphology following treatment with PFN or pneumolysin for the times indicated. Arrows mark invaginated membrane in the case of PFN and blebbed (exvaginated) membrane in the case of pneumolysin.

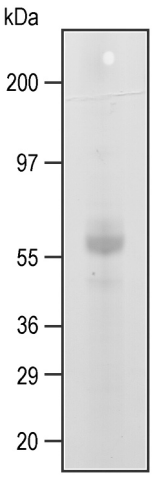

Fig. S7. A silver-stained gel of PFN used in the experiments reported in this paper.

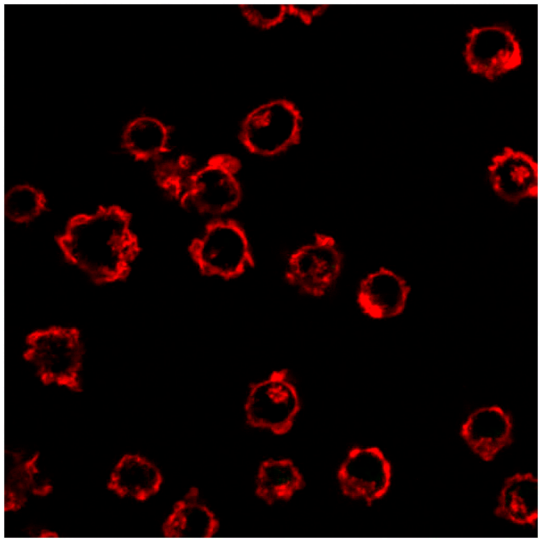

Movie S1. PFN added directly to Jurkat cells shows membrane infolding (red stained) prior to SYTOX Green entry (green).

Movie S1 (AVI)

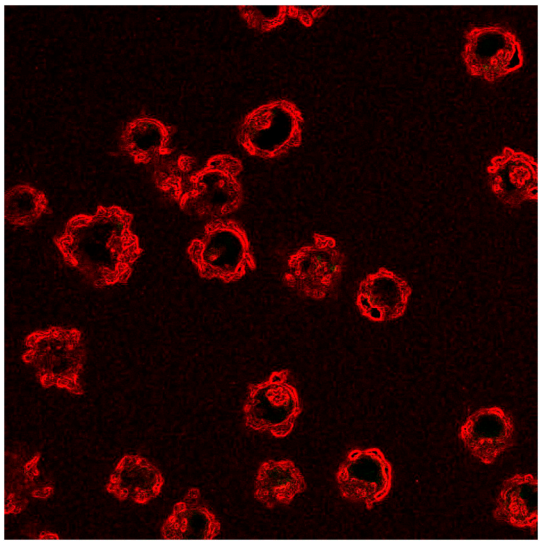

Movie S2. PFN added directly to Jurkat cells shows membrane infolding (red stained) prior to SYTOX Green entry (green). Edge enhanced to emphasize membrane regions.

Movie S2 (AVI)

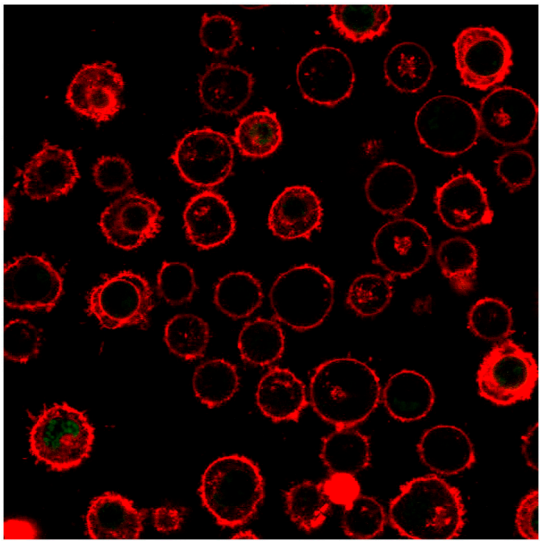

Movie S3. Jurkat cells with PFN added to a final concentration of 1.1 nM show membrane infolding (red stained) prior to SYTOX Green entry (green).

Movie S3 (AVI)

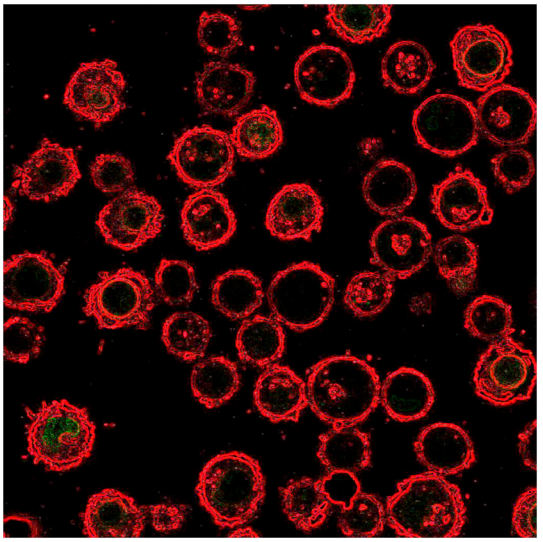

Movie S4. Jurkat cells with PFN added to a final concentration of 1.1 nM show membrane infolding (red stained) prior to SYTOX Green entry (green). Edge enhanced to emphasize membrane regions.

Movie S4 (AVI)

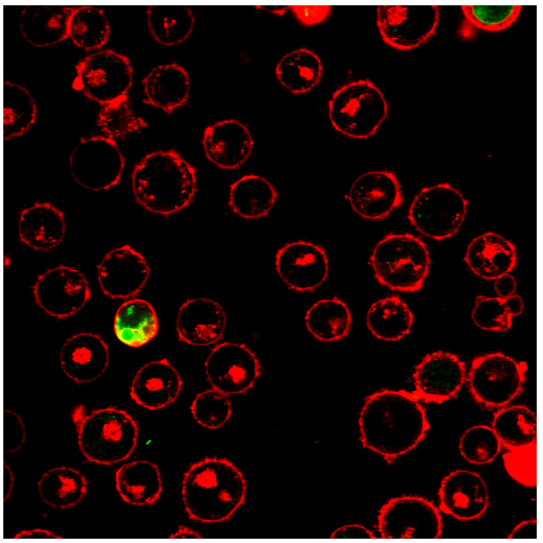

Movie S5. Jurkat cells with PFN added to a final concentration of 1.1 nM with 2 mM EDTA do not show membrane invagination formation.

Movie S5 (AVI)

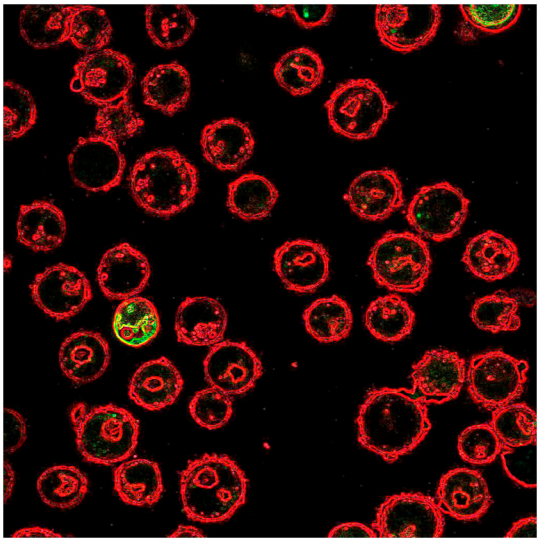

Movie S6. Jurkat cells with PFN added to a final concentration of 1.1 nM with 2 mM EDTA do not show membrane invagination formation. Edge enhanced to emphasize membrane regions.

Movie S6 (AVI)

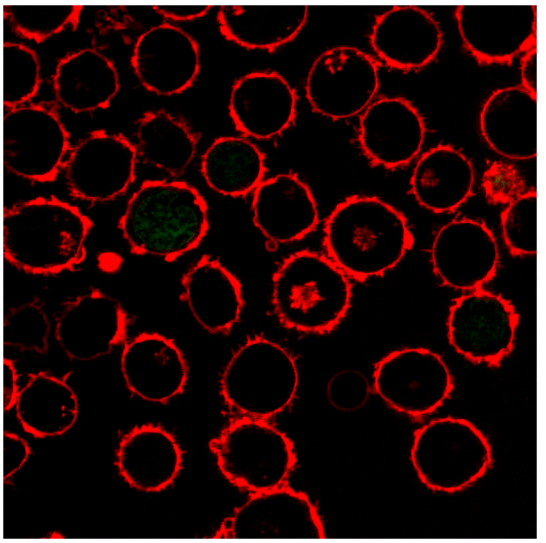

Movie S7. Jurkat cells with pneumolysin added to a final concentration of 0.1 μM show membrane exvagination.

Movie S7 (AVI)

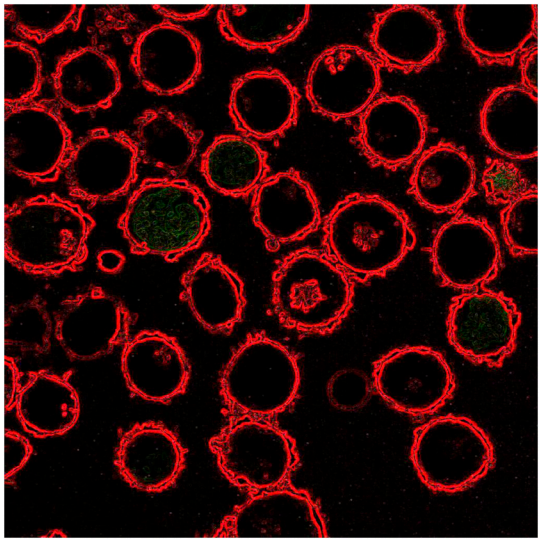

Movie S8. Jurkat cells with pneumolysin added to a final concentration of 0.1 μM show membrane exvagination. Edge enhanced to emphasize membrane regions.

Movie S8 (AVI)

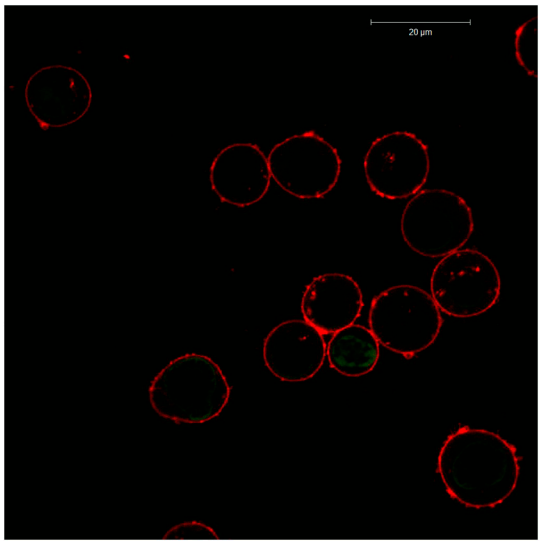

Movie S9. Jurkat cells with lysenin added at 18 μM show pore formation but do not show membrane remodeling (invagination or exvagination).

Movie S9 (AVI)

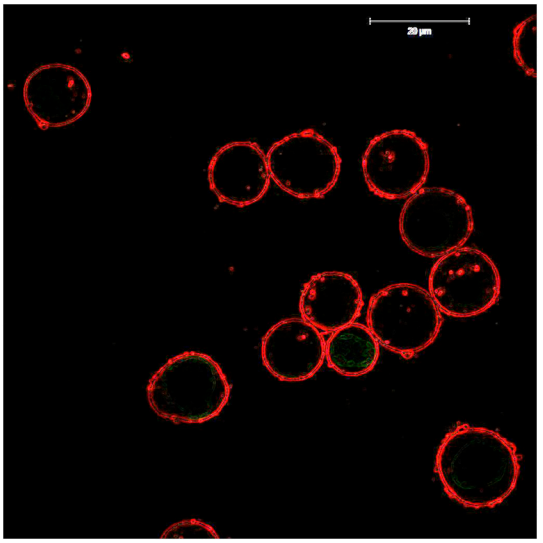

Movie S10. Jurkat cells with lysenin added at 18 µM show pore formation but do not show membrane remodeling (invagination or exvagination). Edge enhanced to emphasize membrane regions.

Movie S10 (AVI)

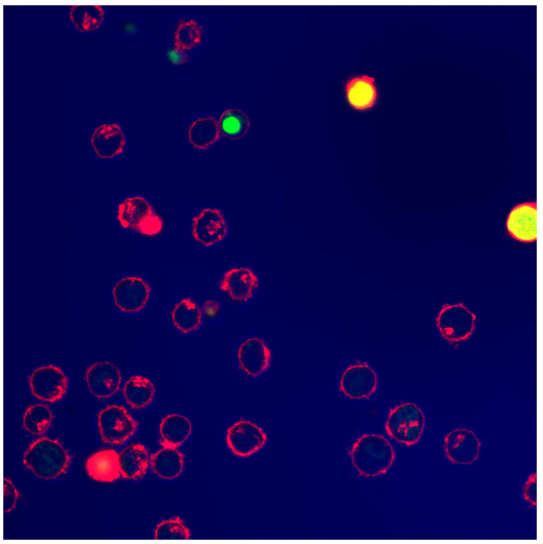

Movie S11. Jurkat cells with rotenone at 0.05 mM.

Movie S11 (AVI)

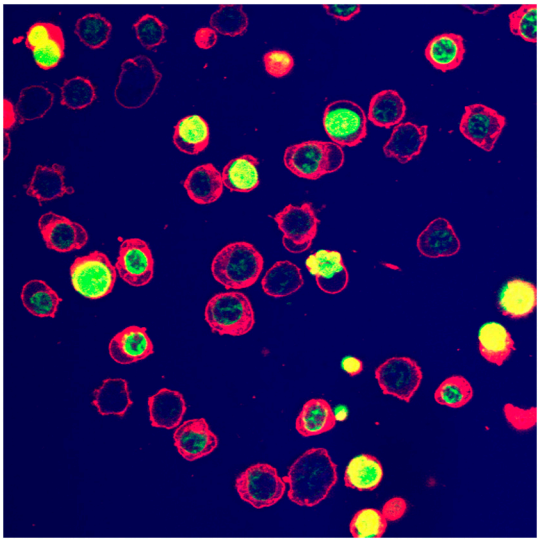

Movie S12. Jurkat cells with rotenone at 0.05 mM and PFN at 0.45 nM.

Movie S12 (AVI)

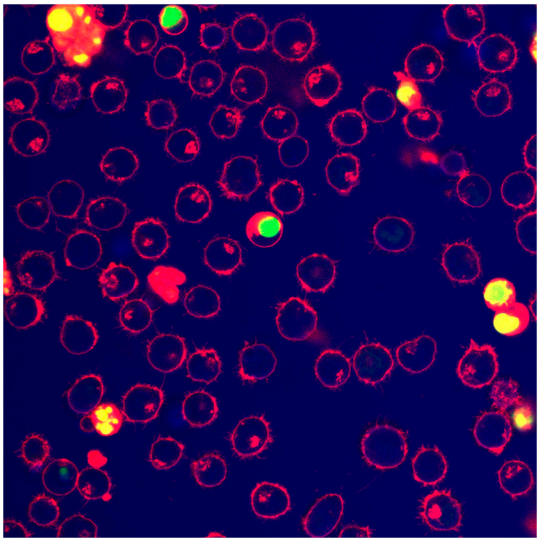

Movie S13. Jurkat cells with azide at 1.625% wt/vol.

Movie S13 (AVI)

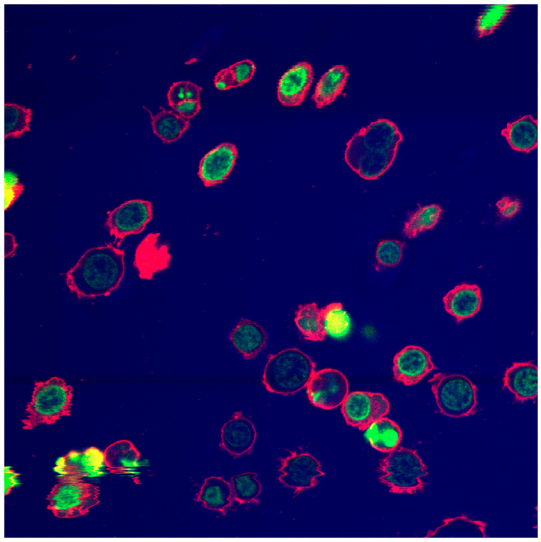

Movie S14. Jurkat cells with azide at 1.625% wt/vol and PFN at 4.5 nM.

Movie S14 (AVI)